



## Get Clarity On Generics

Cost-Effective CT & MRI Contrast Agents

 FRESENIUS  
KABI

[WATCH VIDEO](#)

# AJNR

## Hemorrhage Detected Using MR Imaging in the Setting of Acute Stroke: An In Vivo Model

John Perl II, Jean A. Tkach, Martin Porras-Jimenez, Michael Lieber, Nancy Obuchowski, Jeffrey S. Ross, Xia Ping Ding, Paul M Ruggieri, David M. Shearer, Kaveh Khajavi and Thomas J. Masaryk

This information is current as of August 24, 2025.

*AJNR Am J Neuroradiol* 1999, 20 (10) 1863-1870  
<http://www.ajnr.org/content/20/10/1863>

# Hemorrhage Detected Using MR Imaging in the Setting of Acute Stroke: An In Vivo Model

John Perl II, Jean A. Tkach, Martin Porras-Jimenez, Michael Lieber, Nancy Obuchowski, Jeffrey S. Ross, Xia Ping Ding, Paul M Ruggieri, David M. Shearer, Kaveh Khajavi, and Thomas J. Masaryk

**BACKGROUND AND PURPOSE:** The treatment algorithm for acute cerebrovascular accidents has traditionally sorted these accidents as either hemorrhagic or nonhemorrhagic, and MR imaging, with its ability to allow expeditious assessment of vascular substrates and regional blood volume, is well suited for this purpose. Our purpose was to delineate the accuracy of MR imaging in acute, hemorrhagic forms of stroke during the time frame considered beneficial for intervention in an animal model.

**METHODS:** Eighteen dogs with small, iatrogenic parenchymal, subarachnoid hemorrhage (SAH), or both were serially scanned over the initial 6-hour postictal period. Confirmatory pathologic specimens and 3-hour postictal CT scans were obtained in all animals. The MR and CT studies were then interpreted in a blinded fashion by two neuroradiologists for the presence of hemorrhage. The results were subjected to receiver operating characteristic analysis.

**RESULTS:** MR imaging depicted acute parenchymal hemorrhage and SAH with a high degree of accuracy at 1.5 T. This finding was independent of each of the time points studied during the 6-hour window. For SAH, the MR accuracy for reader 1 was 0.86 (95% CI, 0.76–0.97); for reader 2, accuracy was 0.85 (95% CI, 0.71–0.99). The CT accuracy for the two readers was 0.42 (95% CI, 0.26–0.58) and 0.66 (95% CI, 0.43–0.89), respectively. Fluid-attenuated inversion-recovery images improved the conspicuity of SAH on MR images and, along with spin-density-weighted spin-echo sequences, helped to establish the hemorrhagic nature. For parenchymal hemorrhage, the MR accuracy for reader 1 was 0.90 (95% CI, 0.81–0.99); for reader 2, accuracy was 0.93 (95% CI, 0.84–1.00). With CT, the accuracy of reader 1 was 0.91 (95% CI, 0.85–0.97) whereas for reader 2 accuracy was 0.76 (95% CI, 0.69–0.83). Parenchymal hemorrhage detection and diagnosis was best with T2\*-weighted gradient-echo images.

**CONCLUSION:** MR imaging with appropriately selected sequences appears able to provide information regarding the presence (or absence) of hemorrhage in an acute stroke model requisite to the initiation of treatment.

The treatment algorithm for acute cerebrovascular accidents has traditionally sorted patients on the basis of nonhemorrhagic or hemorrhagic conditions as determined by findings on emergency CT studies (1–6). The recent Food and Drug Administration (FDA) approval and clinical application of thrombolytic therapy for acute stroke has reemphasized

this important distinction, as well as highlighted the need for rapid diagnosis and treatment (7). While additional information (the level of vascular occlusion, viability, and volume of brain at risk) is critical in advancing acute stroke therapy, the time expended acquiring these CT data will delay treatment and possibly exacerbate the injury. MR imaging, with its ability to allow expeditious assessment of the vascular substrate and to acquire dynamic studies of regional blood volume, coupled with diffusion techniques and parenchymal imaging, make it particularly amenable to this application (8, 9). As alternative treatments become available (eg, intra-arterial thrombolysis), efficient and accurate triage of selected patients for particular therapies will require such ancillary data (10).

Nevertheless, the sensitivity of MR imaging for the detection of acute intra- and extra-axial blood during the narrow therapeutic window remains paramount and is still open to question. To date, this

Received December 18, 1998; accepted after revision May 10, 1999.

From the Departments of Diagnostic Radiology (J.P., J.A.T., M.P.-J., M.L., N.O., J.S.R., X.P.D., P.M.R., T.J.M.), Neurosurgery (D.M.S., K.K.), and Biostatistics (M.L., N.O.), Cleveland Clinic Foundation, Cleveland, OH.

Supported in part by National Institutes of Health grant 1RO2HL 43812-01A1.

Address reprint requests to Thomas J. Masaryk, MD, Department of Radiology, Desk Hb6, Cleveland Clinic Foundation, 9500 Euclid Ave, Cleveland, OH 44195.

© American Society of Neuroradiology

**TABLE 1: Diagnostic accuracy of MR imaging for detecting subarachnoid hemorrhage (SAH)**

Time	No. with SAH	No. without SAH	Accuracy* (95% CI)	No. of True-Positive Findings (Sensitivity, %)	No. of True-Negative Findings (Specificity, %)
<b>Reader 1</b>					
Baseline	2	16	0.41 (0.31–0.51)	0/2 (0)	13/16 (81)
0 hour	11	6	0.96 (0.87–1.00)	10/11 (91)	6/6 (100)
1 hour	11	6	0.91 (0.79–1.00)	9/11 (82)	6/6 (100)
2 hours	12	6	0.79 (0.65–0.94)	7/12 (58)	6/6 (100)
4 hours	11	6	0.82 (0.67–0.97)	7/11 (64)	6/6 (100)
6 hours	10	4	0.85 (0.70–1.00)	7/10 (70)	4/4 (100)
<i>Overall†</i>	55	28	<i>0.86 (0.76–0.97)</i>	<i>40/55 (73)</i>	<i>28/28 (100)</i>
<b>Reader 2</b>					
Baseline	2	16	0.28 (0.16–0.41)	0/2 (0)	9/16 (56)
0 hour	11	6	0.91 (0.79–1.00)	9/11 (82)	6/6 (100)
1 hour	11	6	0.76 (0.54–0.98)	8/11 (73)	4/6 (67)
2 hours	12	6	0.84 (0.68–1.00)	9/12 (75)	5/6 (83)
4 hours	11	6	0.86 (0.73–1.00)	8/11 (73)	6/6 (100)
6 hours	10	4	0.90 (0.77–1.00)	8/10 (80)	4/4 (100)
<i>Overall†</i>	55	28	<i>0.85 (0.71–0.99)</i>	<i>42/55 (76)</i>	<i>25/28 (89)</i>

\* Nonparametric estimate of the area under the ROC curve.

† The overall estimate does not contain the baseline data.

issue has been addressed by retrospective analyses of studies in patients presenting with acute focal deficits, only a fraction of whom were evaluated within the therapeutic window and none of whom were administered thrombolytics on the basis of the MR studies alone (11–13). The purpose of this study was to investigate the combined sensitivity and specificity of conventional spin-echo (SE) T1-weighted, spin-density (SD)-weighted, T2/T2\*-weighted gradient-echo (GRE), and fluid-attenuated inversion-recovery (FLAIR) MR sequences to small amounts of parenchymal and subarachnoid hemorrhage (SAH) during the first 6 hours in an *in vivo* animal model.

## Methods

Eighteen mongrel dogs were examined: 12 with iatrogenic SAH, six with parenchymal hematomas in one or both hemispheres, and three with both. Animal Care Committee approval was obtained before the start of the investigation.

Anesthesia induction was with thiopental 20 mg/kg IV (50 mg/mL concentration) to effect. The parenchymal hemorrhage was created by injecting fresh arterial autologous blood (1 mL) into the brain parenchyma through a burr hole using a 22-gauge spinal needle. SAH was created by injecting 2 mL of arterial blood mixed with 2 mL of autologous CSF with a 22-gauge spinal needle inserted into the subarachnoid space through a cisternal puncture. The volume of iatrogenically introduced blood was intentionally small so as to minimize anatomic distention due to gross mass effect. The animals were euthanized at the completion of the 6-hour imaging protocol. Postmortem examination was performed in each animal to confirm the location(s) of the iatrogenic hemorrhage.

MR imaging was performed with a 1.5-T whole-body unit. The animals were imaged in the supine position using a clinical transmit/receive head coil at the following intervals: before hemorrhage (baseline), immediately after ictus, and at 1, 2, 4, and 5½ hours after ictus. Each MR study was completed within a half hour and consisted of a conventional T1-weighted SE sequence, a conventional double-echo SD/T2-weighted SE se-

quence, a fast FLAIR sequence, and a T2\*-weighted GRE sequence. Contiguous axial images were acquired in an interleaved fashion using acquisition parameters similar to those used in human clinical protocols (see Table 1). A noncontrast CT study was also performed 3 hours after ictus with the following parameters: 5-mm section thickness, 140 Kv, 274 to 360 mA, 1.5-second scan cycle, 140-mm field of view, and  $512 \times 512$  matrix.

All 108 MR examinations were interpreted in a random fashion by two neuroradiologists who were blinded to the animal's identity, the presence or absence of intervention, and the time the scan was acquired relative to iatrogenic ictus. The location, size, and signal of all imaging abnormalities and the diagnosis (presence or absence of blood) were recorded, as was the contribution of each MR pulse sequence to the interpretation in view of the expected findings predicted from prior retrospective studies (11, 14–16). More specifically, parenchymal hemorrhage was expected as a heterogeneous mass with a ring-like area of low signal intensity relative to adjacent brain parenchyma on both T1- and T2-weighted images, possibly with a surrounding area of high signal edema on T2-weighted studies. Arterial SAH was expected to be higher in signal intensity than CSF on T1-weighted SE and GRE images as well as on SD and FLAIR sequences, but lower in signal intensity relative to CSF on T2-weighted images. This may be regarded as a complete or partial reversal of the expected CSF/parenchymal contrast that often results in blurring of the CSF/brain interface.

The interpreters assessed each image with respect to parenchymal hemorrhage and SAH, and expressed their confidence in each diagnosis as a percentage (0% to 100%). These data were subsequently analyzed in terms of diagnostic accuracy by measuring the area under the receiver operating characteristic (ROC) curve. Nonparametric estimates of the ROC area were computed (17). To estimate the ROC area for parenchymal hemorrhage, a hemisphere rather than a subject was considered the unit of observation, as with SAH. In computing the ROC area for parenchymal hemorrhage, we compared hemispheres with parenchymal hemorrhage to hemispheres without parenchymal hemorrhage (including SAH). Similarly, in computing the ROC area for SAH, we compared animals with SAH to animals without SAH (including animals with parenchymal hemorrhage). To accommodate the correlation of parenchymal

**TABLE 2: Diagnostic accuracy of MR imaging for detecting parenchymal hemorrhage**

Time	No. with Parenchymal Hemorrhage*	No. without Parenchymal Hemorrhage*	Accuracy† (95% CI)	No. of True-Positive Findings (Sensitivity, %)	No. of True-Negative Findings (Specificity, %)
<b>Reader 1</b>					
Baseline	0	36	...	...	35/36 (97)
0 hour	12	22	0.87 (0.76–0.99)	10/12 (83)	20/22 (91)
1 hour	13	21	0.89 (0.79–0.99)	12/13 (92)	18/21 (86)
2 hours	13	23	0.92 (0.83–1.00)	12/13 (92)	21/23 (91)
4 hours	13	21	0.91 (0.82–1.00)	12/13 (92)	19/21 (91)
6 hours	9	19	0.92 (0.80–1.00)	8/9 (89)	18/19 (95)
<i>Overall‡</i>	<i>60</i>	<i>106</i>	<i>0.90 (0.81–0.99)</i>	<i>54/60 (90)</i>	<i>96/106 (91)</i>
<b>Reader 2</b>					
Baseline	0	36	...	...	35/36 (97)
0 hour	12	22	0.89 (0.78–1.00)	10/12 (83)	20/22 (91)
1 hour	13	21	0.92 (0.82–1.00)	12/13 (92)	18/21 (86)
2 hours	13	23	0.95 (0.87–1.00)	12/13 (92)	20/23 (87)
4 hours	13	21	0.93 (0.83–1.00)	12/13 (92)	19/21 (91)
6 hours	9	19	0.94 (0.83–1.00)	8/9 (89)	18/19 (95)
<i>Overall‡</i>	<i>60</i>	<i>106</i>	<i>0.93 (0.84–1.00)</i>	<i>54/60 (90)</i>	<i>95/106 (90)</i>

\* Denotes number of hemispheres.

† Nonparametric estimate of the area under the ROC curve.

‡ The overall estimate does not contain the baseline data.

hemorrhage test results between hemispheres within a subject, we applied a nonparametric analysis for clustered ROC curve data (18). For all analyses, we used a significance level of .05 (ie, 95% CI). Individual pulse sequences were rated as to their contribution to each diagnosis (in addition to the above-described diagnostic accuracy confidence ratings). Data on the contribution of each MR imaging sequence to the detection and diagnosis were analyzed by Friedman's  $\chi^2$ -test.

The area under the ROC curve was interpreted as the probability that a randomly chosen subject with SAH (or random hemisphere with parenchymal hemorrhage) would be scored with greater suspicion than would a randomly chosen subject (or hemisphere) without SAH (or parenchymal hemorrhage). If MR imaging has no ability to show the distinction between SAH (or parenchymal hemorrhage) and a non-SAH (or nonparenchymal hemorrhage), then the ROC area would theoretically be 0.5. If the CI for the true ROC area contains 0.5, then there is insufficient evidence that the diagnostic technique in question is any better than, for example, a coin flip. In addition, the diagnostic accuracies of MR imaging and CT in the detection of SAH were statistically compared via the  $z$ -test. A similar comparison between MR imaging and CT for parenchymal hemorrhage was also performed.

CT scans were interpreted blindly in the usual fashion; blood proteins were expected to appear as an area of high-attenuation coefficient in the subarachnoid space or brain parenchyma, depending on the location of the hemorrhage (19–21). As with the interpretation of the MR studies, interpretations of the 3-hour CT scans were subjected to the same ROC analysis (17, 18).

## Results

Postmortem examination confirmed the presence of parenchymal hemorrhage or SAH or both in each subject. Tables 1 and 2 summarize, by reader, the results of the diagnostic accuracy of the MR study. Several studies were interrupted because of inadequate anesthesia or subject motion (hence, the variability of  $n$  at each time point). In Table 1, es-

timates of diagnostic accuracy for detecting SAH are given; Table 2 shows estimates of diagnostic accuracy for detecting parenchymal hemorrhage. The results are summarized at each time point and then pooled to produce an overall estimate of diagnostic accuracy within the therapeutic window. In addition to the estimates of diagnostic accuracy, the tables also give the number of observations at each time point, the number of observations in which the reader indicated some (ie, >0%) confidence in the presence of SAH (Table 1) or parenchymal hemorrhage (Table 2), and the average confidence score for those cases.

In Table 1, for reader 1 at baseline, two subjects have SAH and 16 do not. In the two subjects with SAH, the reader did not detect (at any confidence level) the SAH, so there are no true-positive scores out of a possible two. In the 16 cases without SAH, the reader assigned some confidence to the presence of SAH in three cases (average confidence score, 60.0). Thus, at baseline, the 95% CI for the ROC area for reader 1 does contain 0.5, and the 95% CI for reader 2 is completely below 0.5. Note that (for either reader) the 95% CI for time points 0 hour, 1 hour, 2 hours, 4 hours, and 6 hours do not contain 0.5. Therefore, for these time points, MR imaging is significantly better than chance for predicting the presence of SAH.

The overall estimate of diagnostic accuracy for detecting SAH (excluding baseline) was 0.86 for reader 1 (95% CI, 0.76–0.97) and 0.85 for reader 2 (95% CI, 0.71–0.99). In other words, we are 95% confident that reader 1 is able to distinguish SAH from non-SAH 76% to 97% of the time, and that reader 2 is able to make this distinction 71% to 99% of the time. For each reader, we also tested



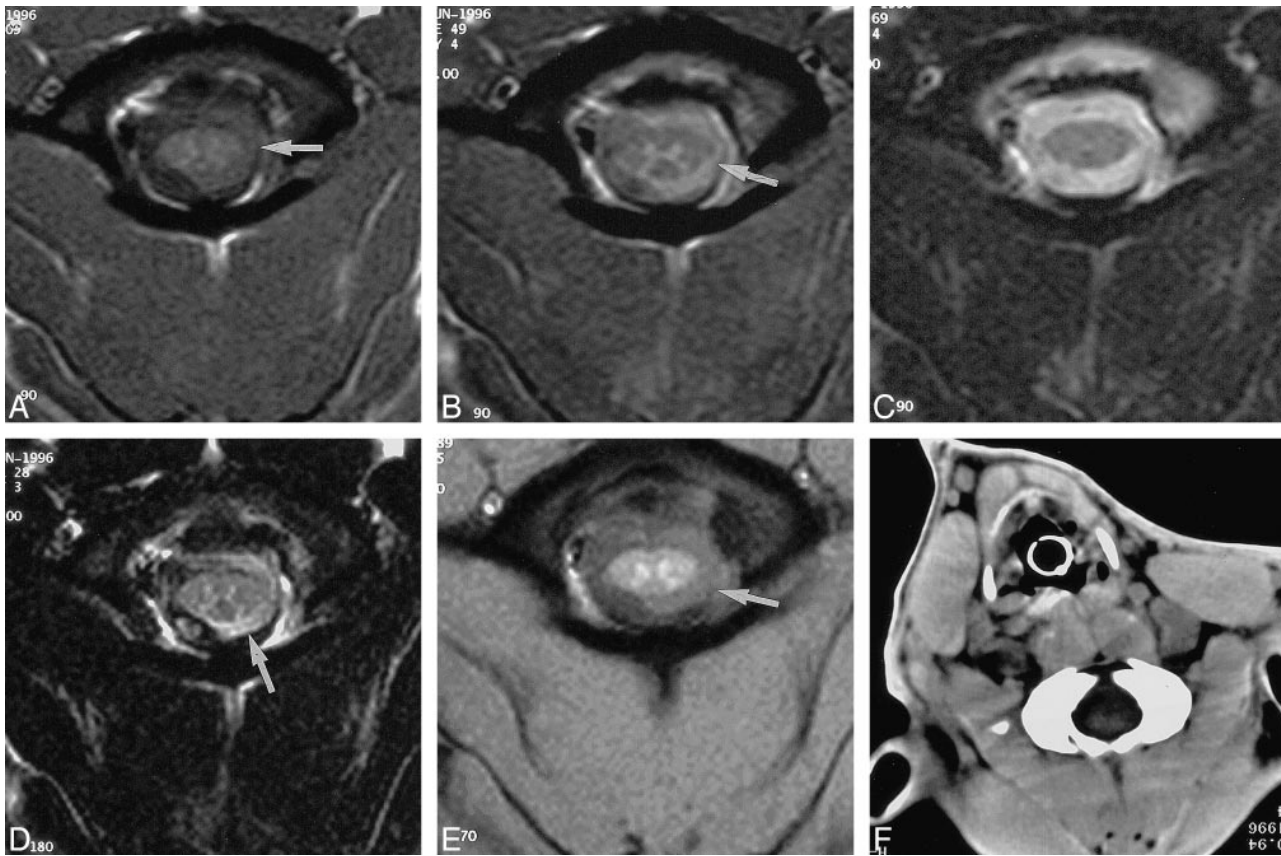


FIG 1. A–F, T1-weighted (A), SD-weighted (B), T2-weighted (C), FLAIR (D), and GRE (E) MR images and CT scan (F) of SAH at the level of the cervicomedullary junction in the same canine. Blood is seen on the MR images (obtained 2 hours after ictus) as an area of high signal obscuring the CSF-brain interface on the left (arrows). This is most conspicuous on the FLAIR image (D) and is not seen to any significant degree on the T2-weighted image (C) or the CT scan (F), performed 1 hour later.

whether the diagnostic accuracy at the 0-hour time point differed from the diagnostic accuracy at the 6-hour time point. The differences were not statistically significant at the .05 level (reader 1:  $P = .07$ ; reader 2:  $P = 1.00$ ).

In Table 2, the diagnostic accuracy for detecting parenchymal hemorrhage at baseline could not be estimated, since there were no hemispheres with parenchymal hemorrhage. After baseline, all the ROC areas could be estimated; neither of the 95% CIs for the two readers contained 0.5, indicating that MR imaging is better than chance for predicting presence or absence of parenchymal hemorrhage. Also, as with the SAH data, the results were pooled across the five time points for each reader to arrive at an overall estimate of diagnostic accuracy for detecting parenchymal hemorrhage. Excluding baseline, this was 0.90 for reader 1 (95% CI, 0.81–0.99) and 0.93 for reader 2 (95% CI, 0.84–1.00). In other words, we are 95% confident that reader 1 is able to distinguish parenchymal from nonparenchymal hemorrhage 81% to 99% of the time, and that reader 2 is able to make this distinction 84% to 100% of the time. For each reader, we also tested the diagnostic accuracy at the 0-hour time point against that at the 6-hour time point. The differ-

ences in diagnostic accuracy were not statistically significant (reader 1:  $P = .19$ ; reader 2:  $P = .18$ ).

Also measured were the relative contributions of each scan/pulse sequence to the diagnosis of SAH and parenchymal hemorrhage (Figs 1 and 2, respectively). With SAH, lesion detection was much better with fast FLAIR, but the conventional SD-weighted SE and T2\*-weighted GRE sequences were also important in establishing the hemorrhagic diagnosis (Fig 1). For the SAH studies, the conventional T1- and T2-weighted SE images frequently failed to provide any useful information for detection or diagnosis. Parenchymal hemorrhage was identified in every canine at least at one time point by MR imaging. In the case of parenchymal hemorrhage, the T2\*-weighted GRE sequences were most helpful for the detection and diagnosis of lesions (Fig 2). For the detection of lesions, the fast FLAIR images were the second most helpful, but for diagnosis, the T2-weighted SE images were the second most helpful. Conversely, the conventional T1- and SD-weighted SE images were found not to be beneficial in the evaluation of parenchymal hemorrhage. These findings were consistent, independent of the time at which the images were acquired relative to the time of hemorrhage crea-

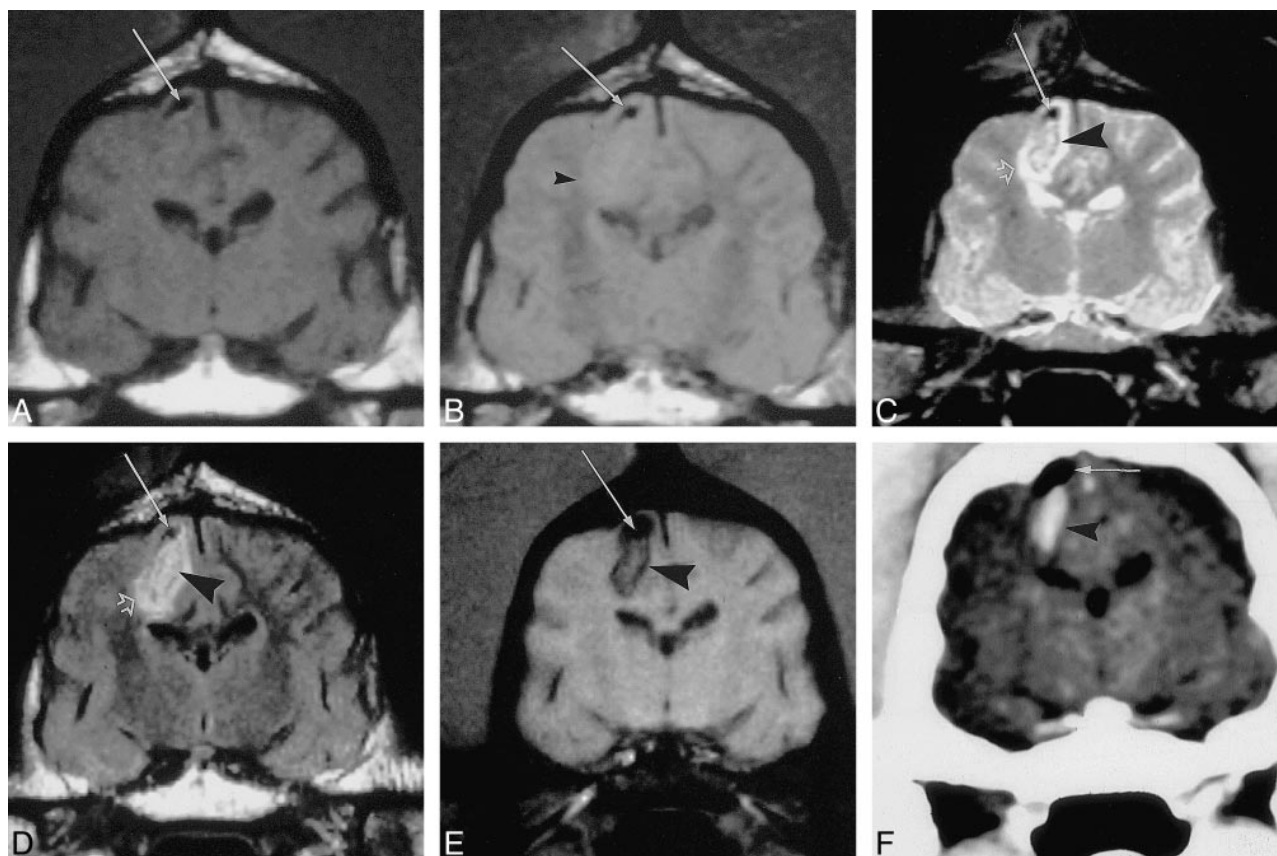


FIG 2. A–F, T1-weighted (A), SD-weighted (B), T2-weighted (C), FLAIR (D), and GRE (E) MR images and CT scan (F) of parenchymal hemorrhage within the right hemisphere in the same canine. All MR studies were performed 2 hours after ictus and show a focus of low-signal susceptibility artifact near the vertex, which, on the 3-hour CT scan, is found to be iatrogenically introduced gas (arrow). The T1-weighted image (A) does not show the parenchymal hemorrhage, whereas the SD-weighted image shows only vague loss of the gray/white junction (arrowhead, B). T2-weighted (C) and FLAIR (D) images display the heterogeneous hematoma with a ring of low signal (arrowhead) surrounded by vasogenic edema (open arrow). GRE image (E) prominently shows only heterogeneous susceptibility effect in the area of the hematoma (arrowhead), while CT scan shows the typical high-attenuation mass (F).

tion. An example of false-negative detection appears in Figure 3.

Tables 3 and 4 summarize the results of the diagnostic accuracy aspect of the CT studies obtained by readers 1 and 2. In Table 3, the estimates of diagnostic accuracy for detecting SAH are given; Table 4 shows the estimates of diagnostic accuracy for detecting parenchymal hemorrhage. The overall estimate of diagnostic accuracy for detecting SAH was 0.42 for reader 1 (95% CI, 0.26–0.58) and 0.66 for reader 2 (95% CI, 0.43–0.89). Hence, we are 95% confident that reader 1 is able to distinguish SAH from non-SAHA 26% to 58% of the time, and that reader 2 is able to make this distinction 43% to 89% of the time (Fig 1). Note that (for both readers) the 95% CIs contain 0.5. Thus, in this instance, there is no evidence that CT was useful (ie, significantly better than guessing) in distinguishing non-SAHA from SAHA in this animal model.

For reader 1, the difference in accuracy between MR imaging (0.79) and CT (0.42) in detecting SAH was statistically significant ( $P < .001$ ,  $z$ -test). However, for reader 2, the difference in accuracy between MR imaging and CT (0.84 versus 0.66) in

detecting SAH was not statistically significant ( $P = .12$ ,  $z$ -test).

Table 4 shows the diagnostic accuracy of CT for detecting parenchymal hemorrhage. For both readers, the 95% CIs do not contain 0.5; thus, CT is significantly better than guessing for predicting the presence or absence of parenchymal hemorrhage. The overall estimate of diagnostic accuracy for detecting parenchymal hemorrhage was 0.91 for reader 1 (95% CI, 0.85–0.97) and 0.76 for reader 2 (95% CI, 0.69–0.83) (Fig 2).

For reader 1, the difference between MR imaging (0.90) and CT (0.91) in detecting parenchymal hemorrhage was not statistically significant ( $P = .74$ ,  $z$ -test); for reader 2, the difference between MR imaging (0.93) and CT (0.76) was significant ( $P < .001$ ,  $z$ -test).

### Discussion

In 1995, the rt-PA Study Group of the National Institute of Neurologic Disorders and Stroke (NINDS) reported improved outcomes at 90 days in patients with presumed ischemic stroke treated

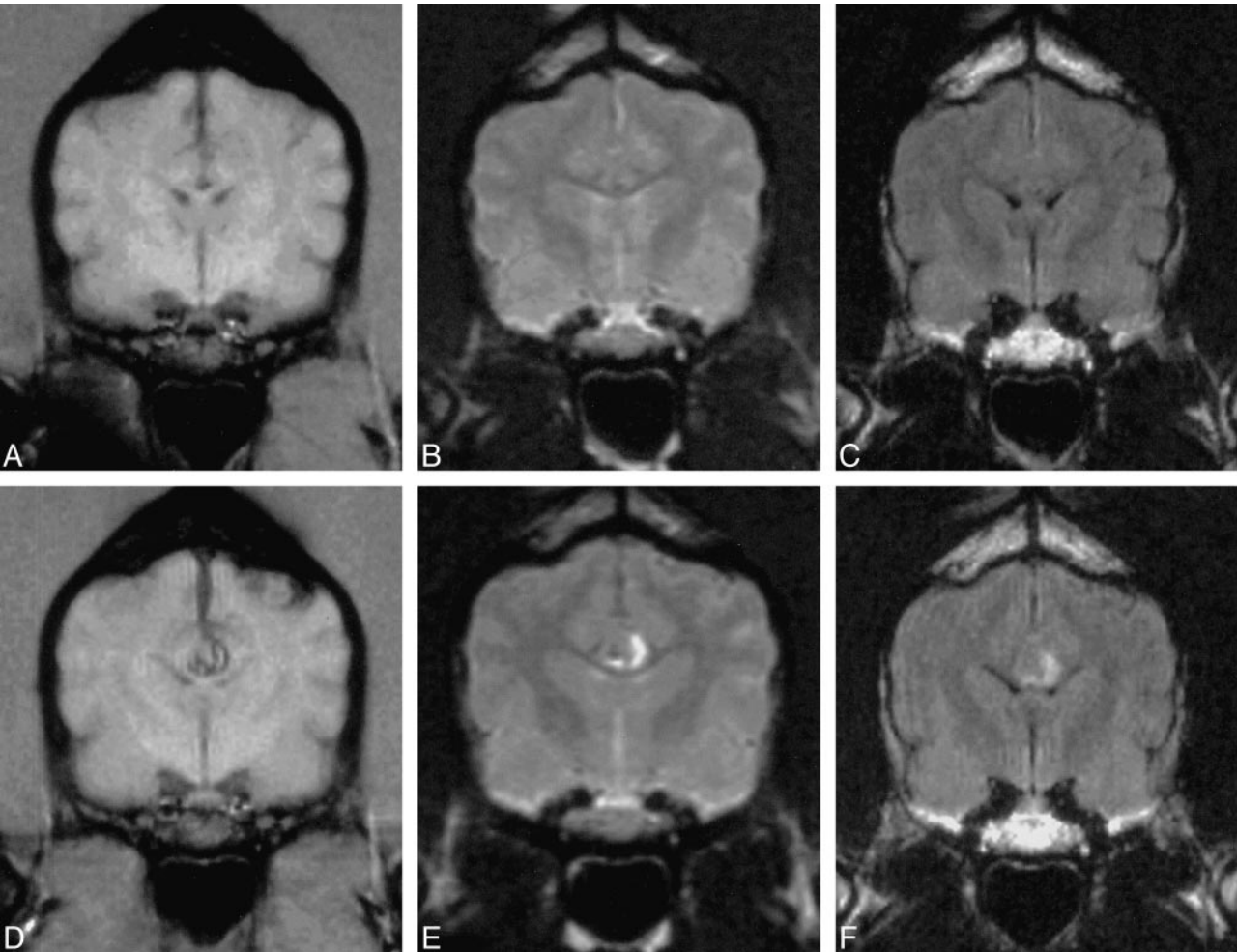


FIG 3. Hyperacute parenchymal hemorrhage.

A–C, T1-weighted (A), T2-weighted (B), and FLAIR (C) MR images obtained immediately after creation of parenchymal hemorrhage show a false-negative abnormality not detected by either reader.

D–F, T1-weighted (D), T2-weighted (E), and FLAIR (F) MR images in the same animal 1 hour after creation of the hemorrhage show the obvious abnormality in the area of the corpus callosum, consistent with hyperacute parenchymal hemorrhage. All abnormalities were detected by both readers on all sequences.

TABLE 3: Diagnostic accuracy of CT for detecting SAH

	No. with SAH	No without SAH	Accuracy* (95% CI)	No. of True-Positive Findings (Sensitivity, %)	No. True-Negative Findings (Specificity, %)
Reader 1	12	6	0.42 (0.26–0.58)	0/12 (0)	5/6 (83)
Reader 2	12	6	0.66 (0.43–0.89)	6/12 (50)	5/6 (83)

\* Nonparametric estimate of the area under the ROC curve.

TABLE 4: Diagnostic accuracy of CT for detecting parenchymal hemorrhage

	No. with Parenchymal Hemorrhage*	No. without Parenchymal Hemorrhage*	Accuracy† (95% CI)	No. of True-Positive Findings (Sensitivity, %)	No. of True-Negative Findings (Specificity, %)
Reader 1	13	23	0.91 (0.85–0.97)	10/13 (77)	21/23 (91)
Reader 2	13	23	0.76 (0.69–0.83)	7/13 (54)	21/23 (91)

\* Denotes number of hemispheres.

† Nonparametric estimate of the area under the ROC curve.



with intravenous rt-PA within 3 hours of the onset of symptoms. On the basis of these findings, the FDA subsequently approved the use of rt-PA for the treatment of acute stroke (7). Because of the 3-hour time-to-treat constraint imposed by the study protocol, pretreatment imaging was limited to CT in order to exclude patients with a possible hemorrhagic component to their neurologic deficit. Conversely, this and previous work suggest that additional diagnostic information (eg, the site and size of vessel occlusion, the extent of infarction, and the residual viability of adjacent brain parenchyma) may be helpful in optimizing present treatment regimens and in defining those of the future (10, 22–25). In this context, interest has been directed toward considering the feasibility of a single expeditious diagnostic examination. MR imaging and dynamic spiral CT scanning have both been proposed as possible alternatives to simple, unenhanced axial CT of the brain parenchyma. While CT traditionally has afforded the ability to image the brain parenchyma along with the potential to examine the vasculature and blood flow (26, 27), MR imaging has been viewed as particularly appealing owing to the high sensitivity of diffusion-weighted imaging to the early changes of cytotoxic edema in addition to the capacity to delineate vascular anatomy and physiology (8, 9, 12, 25, 28–30).

As thrombolysis is the only proved therapy for acute stroke, but is associated with an increased risk of intracranial hemorrhage, the exclusion of an underlying hemorrhage remains paramount. Owing to the multiplicity of available MR techniques as well as the evolutionary MR appearance of blood products at various field strengths, the sensitivity of MR imaging to hemorrhage has never had the same simple black/white distinction (literally) that has characterized CT. Recent retrospective clinical reports have suggested that carefully performed MR examinations may possess the necessary sensitivity to parenchymal hemorrhage to allow its expeditious, and exclusive, use in the evaluation of acute cerebrovascular events (11, 13). Recent reports indicate that the signal-intensity pattern is consistent with magnetic susceptibility effects of paramagnetic deoxygenated hemoglobin within intact erythrocytes (31).

The results of the present study show that MR imaging can show acute parenchymal hemorrhage and SAH with a high degree of sensitivity in an in vivo model in the time frame presently considered effectual for acute stroke intervention. FLAIR images improve the conspicuity of the SAH lesion on MR images and, along with SD-weighted SE images, help to establish the hemorrhagic nature of the lesion. For parenchymal hemorrhage, detection and diagnosis is best with T2\*-weighted GRE images. Additional optimization of FLAIR sequences, to reduce CSF flow artifacts, and implementation of volume GRE imaging, with its improved spatial coverage, may improve this sensitivity.

In this study, the sensitivity of a tailored MR examination to parenchymal hemorrhage appears to be at least comparable to that provided by CT within the first few hours after ictus. Clearly, as the European Cooperative Acute Stroke Study demonstrated, the inability to diagnose completed ischemic infarction accurately may impact patient outcome, as might the catastrophic misdiagnosis of the far less common parenchymal hemorrhage in a patient treated with thrombolytics (1, 2).

Somewhat unexpected were the results of the MR and CT studies performed in subjects with SAH. In retrospect, these results are not surprising, and may reflect interpretive bias relative to MR imaging and limitations in the design of the animal model relative to CT. In particular, prior to this study, CT was (and has remained) the imaging examination of choice for acute cerebrovascular events at our institution, in large part because of our active participation in prospective stroke treatment protocols, which dictate the screening examination (10). The lack of experience with routine clinical MR examination of acute SAH may have played a role in what appears to be the overzealous interpretation of the baseline MR images. Additionally, the model consisted of injecting a relatively small amount (2 mL) of autologous blood into a small subarachnoid space surrounded by the dense bone of the canine posterior fossa. These conditions are remote from clinical practice and, when coupled with the presence of beam-hardening artifacts, become unfavorable to the diagnostic capabilities of CT. In practice, the extent of bleeding necessary to produce a clinical picture of stroke consistent with either SAH or bland infarction (ie, a higher Hunt-Hess grade or a total neurologic deficit of less than 4 on the National Institute of Health Stroke Scale) is unlikely to be ignored by either technique on the basis of tissue contrast and such secondary signs as mass effect and hydrocephalus.

## Conclusion

In the setting of significant time constraints, the potential of future therapies in the form of alternative routes of administration (10) and neuroprotective agents (24, 32–34) will require more objective diagnostic data in order to guide therapy rationally (35). MR imaging alone, with appropriately selected sequences, appears able to provide the requisite information for the initiation of treatment.

## References

1. Schrager DL, Kalafut M, Starkman S, Krueger M, Saver JL. **Cranial computed tomography interpretation in acute stroke: physician accuracy in determining eligibility for thrombolytic therapy.** *JAMA* 1998;279:1293–1297
2. von Kummer R, Allen KL, Holle R, et al. **Acute stroke: usefulness of early CT findings before thrombolytic therapy.** *Radiology* 1997;205:327–333



3. von Kummer R, Holle R, Gizyska U, et al. **Interobserver agreement in assessing early CT signs of middle cerebral artery infarction.** *AJNR Am J Neuroradiol* 1996;17:1743-1748
4. von Kummer R, Meyding-Lamade U, Forsting M, et al. **Sensitivity and prognostic value of early CT in occlusion of the middle cerebral artery trunk.** *AJNR Am J Neuroradiol* 1994;15:9-15
5. von Kummer R, Weber J. **Brain and vascular imaging in acute ischemic stroke: the potential of computed tomography.** *Neurology* 1997;49:S52-S55
6. von Kummer R. **Thrombolysis in acute ischemic stroke: a two-fold challenge for the neuroradiologists.** *Riv Neuroradiol* 1996;9:29-34
7. NINDS rt-PA Investigators. **Tissue plasminogen activator for acute ischemic stroke.** *N Engl J Med* 1995;333:1581-1587
8. Russell EJ. **Diagnosis of hyperacute ischemic infarct with CT: key to improved clinical outcome after intravenous thrombolysis?** *Radiology* 1997;205:315-318
9. Brant-Zawadzki M. **CT angiography in acute ischemic stroke: the right tool for the job?** *AJNR Am J Neuroradiol* 1997;18:1021-1023
10. PROACT II Investigators. **Recombinant pro urokinase (r-Pro UK) in acute cerebral thromboembolism: initial trial results.** *Stroke* 1999;30:234
11. Patel MR, Edelman RR, Warach S. **Detection of hyperacute primary intraparenchymal hemorrhage by magnetic resonance imaging.** *Stroke* 1996;27:2321-2324
12. Sorensen AG, Buonanno FS, Gonzalez RG, et al. **Hyperacute stroke: evaluation with combined multisection diffusion-weighted and hemodynamically weighted echo-planar MR imaging.** *Radiology* 1996;199:391-401
13. Schellinger PD, Hansen O, Fiebach JB, Hacke W, Sartor K. **A standardized MRI stroke protocol: comparison with CT in hyperacute intracerebral hemorrhage.** *Stroke* 1999;30:765-768
14. Noguchi K, Ogawa T, Inugami A, et al. **Acute subarachnoid hemorrhage: MR imaging with fluid-attenuated inversion recovery pulse sequences.** *Radiology* 1995;196:773-777
15. Noguchi K, Ogawa T, Seto H, et al. **Subacute and chronic subarachnoid hemorrhage: diagnosis with fluid-attenuated inversion-recovery MR imaging.** *Radiology* 1997;203:257-262
16. Atlas SW, Mark AS, Grossman RI, Gomori JM. **Intracranial hemorrhage: gradient-echo MR imaging at 1.5 T. Comparison with spin-echo imaging and clinical applications.** *Radiology* 1988;168:803-807
17. Hanley JA, McNeil BJ. **The meaning and use of the area under a receiver operating characteristic (ROC) curve.** *Radiology* 1982;143:29-36
18. Obuchowski NA. **Nonparametric analysis of clustered ROC curve data.** *Biometrics* 1997;53:567-578
19. Scotti G, Ethier R, Melancon D, Terbrugge K, Tchang S. **Computed tomography in the evaluation of intracranial aneurysms and subarachnoid hemorrhage.** *Radiology* 1977;123:85-90
20. New PF, Aronow S. **Attenuation measurements of whole blood and blood fractions in computed tomography.** *Radiology* 1976;121:635-640
21. Norman D, Price D, Boyd D, Fishman R, Newton TH. **Quantitative aspects of computed tomography of the blood and cerebrospinal fluid.** *Radiology* 1977;123:335-338
22. Wolpert SM, Bruckmann H, Greenlee R, Wechsler L, Pessin MS, del Zoppo GJ. **Neuroradiologic evaluation of patients with acute stroke treated with recombinant tissue plasminogen activator: the rt-PA Acute Stroke Study Group.** *AJNR Am J Neuroradiol* 1993;14:3-13
23. Tomsick T, Brott T, Barsan W, et al. **Prognostic value of the hyperdense middle cerebral artery sign and stroke scale score before ultraearly thrombolytic therapy.** *AJNR Am J Neuroradiol* 1996;17:79-85
24. Beauchamp NJJ, Bryan RN. **Acute cerebral ischemic infarction: a pathophysiologic review and radiologic perspective.** *AJR Am J Roentgenol* 1998;171:73-84
25. Beauchamp NJJ, Ulug AM, Passe TJ, van Zijl PC. **MR diffusion imaging in stroke: review and controversies.** *Radiographics* 1998;18:1269-1283
26. Koenig M, Klotz E, Luka B, Venderink DJ, Spittler JF, Heuser L. **Perfusion CT of the brain: diagnostic approach for early detection of ischemic stroke.** *Radiology* 1998;209:85-93
27. Knauth M, von Kummer R, Jansen O, Hahnel S, Dorfler A, Sartor K. **Potential of CT angiography in acute ischemic stroke.** *AJNR Am J Neuroradiol* 1997;18:1001-1010
28. Warach S, Mosley M, Sorensen AG, Koroshetz W. **Time course of diffusion imaging abnormalities in human stroke.** *Stroke* 1996;27:1254-1256
29. Warach S, Dashe JF, Edelman RR. **Clinical outcome in ischemic stroke predicted by early diffusion-weighted and perfusion magnetic resonance imaging: a preliminary analysis.** *J Cereb Blood Flow Metab* 1996;16:53-59
30. Warach S, Gaa J, Siewert B, Wielopolski P, Edelman RR. **Acute human stroke studied by whole brain echo planar diffusion-weighted magnetic resonance imaging.** *Ann Neurol* 1995;37:231-241
31. Atlas SW, Thulborn KR. **MR detection of hyperacute parenchymal hemorrhage of the brain.** *AJNR Am J Neuroradiol* 1998;19:1471-1477
32. Brint SU. **Acute stroke therapies.** *Surg Neurol* 1996;46:446-449
33. Ginsberg MD. **The new language of cerebral ischemia.** *AJNR Am J Neuroradiol* 1997;18:1435-1445
34. Dyker AG, Lees KR. **Duration of neuroprotective treatment for ischemic stroke.** *Stroke* 1998;29:535-542
35. Redelmeier DA, Shafir E. **Medical decision making in situations that offer multiple alternatives.** *JAMA* 1995;273:302-305